Resonance Assignments and Secondary Structure Analysis of *E. coli* Thioredoxin by Magic Angle Spinning Solid-State NMR Spectroscopy

Dabeiba Marulanda,[†] Maria Luisa Tasayco,*[,‡] Marcela Cataldi,[‡] Vilma Arriaran,[‡] and Tatyana Polenova*[,†]

Department of Chemistry and Biochemistry, Brown Laboratories, University of Delaware, Newark, Delaware 19716, and Department of Chemistry, Science Building, City College of the City University of New York, New York, New York 10031

Received: May 25, 2005; In Final Form: June 24, 2005

De novo site-specific ^{13}C and ^{15}N backbone and sidechain resonance assignments are presented for uniformly enriched *E. coli* thioredoxin, established using two-dimensional homo- and heteronuclear solid-state magic angle spinning NMR correlation spectroscopy. Backbone dihedral angles and secondary structure were derived from the statistical analysis of the secondary chemical shifts, and are in good agreement with solution values for the intact full-length thioredoxin, with the exception of a small number of residues located at the termini of the individual secondary structure elements. A large number of cross-peaks observed in the DARR spectra with long mixing times correspond to the pairs of carbon atoms separated by 4−6 Å, suggesting that DARR could be efficiently employed for observation of medium- and long-range correlations. The 108 amino acid residue *E. coli* thioredoxin is the largest uniformly enriched protein assigned to this degree of completeness by solid-state NMR spectroscopy to date. It is anticipated that with a combination of two-dimensional correlation experiments and high magnetic fields, resonance assignments and secondary structure can be generally derived for other noncrystalline proteins.

Introduction

Solid-state NMR spectroscopy is a powerful technique for analysis of noncrystalline biological materials intractable by other structural methods. Recent studies demonstrate the potential of solids NMR for detailed investigations of complex biological systems, encompassing membrane proteins and peptides,[1−9] amyloid fibrils,[10−12] biomaterials,[13] and intact cells.[14]

With the advances in the experimental methodologies and hardware, high-resolution solid-state NMR spectroscopy for protein structure determination has become an active and rapidly growing area of research. Only several years ago it was not at all clear whether multidimensional solids NMR correlation spectroscopy would be generally feasible or informative for structural analysis of uniformly enriched proteins. However, recent reports from several laboratories suggest that resonance assignments and determination of structural constraints from multidimensional solid-state magic angle spinning spectra of proteins could be successfully accomplished for a number of proteins. Partial or nearly complete resonance assignments have been demonstrated to date for six uniformly enriched proteins, including ubiquitin,[15−19] BPTI,[20] the α-spectrin SH_3 domain,[21] the catabolite repression histidine-containing phosphocarrier protein Crh,[23] reassembled thioredoxin,[24] and the immunoglobulin-binding domain B1 of Streptococcal Protein G (GB1).[25]

The ultimate goal of the above efforts is to establish general experimental methodologies that would enable high-resolution structural studies of uniformly enriched intrinsically noncrystalline biological solids. The initial investigations have focused on soluble proteins, where sample preparation and NMR spectroscopic procedures could be readily optimized. Despite the significant progress in all aspects of protein structure determination protocols by solids NMR, there are still a number of remaining challenges and questions. For example, in contrast to solution NMR, where resonance assignments are performed according to the standard procedures even for fairly large proteins (>15 kDa), the best experimental routes are still a subject of debate within the solid-state NMR community. Moreover, to date complete three-dimensional structures derived from solids NMR experiments have been reported for only two proteins, α-spectrin SH_3 domain and ubiquitin.[21,22] In this system, two sets of ^{13}C isotopically diluted samples were employed to observe a sufficient number of long-range distance restraints otherwise attenuated by dipolar truncation.[26,27] Therefore, it is not clear whether several sets of samples with different isotopic labeling patterns would be generally required in addition to the uniformly ^{13}C,^{15}N-enriched protein for successful 3D structure determination by solid-state NMR. For proteins where *E. coli* expression systems are not feasible, preparation of such extensively enriched samples may be challenging. Another unanswered question is whether the current high-resolution solids NMR protocols for resonance assignments and structure determination are restricted to small proteins, as the largest molecule assigned by solid-state NMR spectroscopy prior to this work had been an 89-residue phosphocarrier protein Crh.[23] In contrast with solution NMR spectroscopy, the resonance linewidths in the solid state are generally independent of the molecular weight. For larger proteins, the increased number of resonances is expected to make the spectral interpretation tedious. However, increasing the dimensionality of the solid-state NMR experi-

* To whom the correspondence should be addressed. T. P.: University of Delaware, phone (302) 831-1968, e-mail tpolenov@chem.udel.edu. M.L.T.: City College of New York, phone (212) 650-8169, e-mail mltj@mafalda.sci.ccny.cuny.edu.

[†] University of Delaware.

[‡] City College of the City University of New York.

10.1021/jp052774d CCC: $30.25
Published on Web 09/01/2005

ments in conjunction with alternative isotopic enrichment strategies[24,28−30] could alleviate the above problem and permit detailed structural analysis of larger proteins by solid-state NMR.

In this report, we present the ^{13}C and ^{15}N chemical shift assignments and secondary structure analysis for a 108-amino acid residue *E. coli* thioredoxin. We discuss that the experimental protocol involving two-dimensional homo- and heteronuclear correlation spectroscopy at high magnetic fields permits assignment of the backbone and the sidechain resonances for 107 residues, with modest amounts of experimental time. We additionally demonstrate that even in the uniformly enriched thioredoxin, a number of meaningful long-range $^{13}C-^{13}C$ correlations could be identified from the DARR spectra, and that attenuation of the long-range cross-peaks due to the dipolar truncation is modest. The *E. coli* thioredoxin is the largest uniformly enriched protein assigned to this degree of completeness by solids NMR spectroscopy to date, and as will be described below, the quality of the spectra suggests that substantially larger uniformly and extensively enriched systems will be amenable to detailed characterization by solid-state NMR.

Experimental Section

Materials. All chemicals were obtained from Sigma. D-[U-$^{13}C_6$]-glucose and [^{15}N]-ammonium chloride were purchased from Cambridge Isotope Laboratories. Biochemicals for bacterial cultures were purchased from Oxoid, Inc. All reagents were used without further purification. The VDX crystallization plates and siliconized cover slips were from Hampton Research.

Expression and Purification of U-^{13}C,^{15}N Enriched *E. coli* Thioredoxin. Overexpression of oxidized wild-type thioredoxin was performed as described previously[31] in *E. coli* JF521 strain (gift of Dr. J. Fuchs and Dr. C. K. Woodward) containing the plasmid pTK100 with the Trx gene. The construct is identical with that used in the previous solution NMR studies by Dyson and co-workers.[32] Overexpression of uniformly labeled oxidized wild-type thioredoxin was performed in *E. coli* BL21(DE3) strain from Novagen using published procedures.[33] Isotopic labels were introduced using M9 minimal medium[34] containing either [^{15}N]-ammonium chloride (1 g/L of minimal medium) together with the natural abundance glucose or D-[U-$^{13}C_6$]-glucose (4 g/L of minimal medium) together with the [^{15}N]-ammonium chloride (1 g/L of minimal media). Purification of the wild-type thioredoxin with and without the NMR labels was done by molecular exclusion and ionic exchange chromatography using published procedures.[35] Characterization of the wild-type thioredoxin was performed using PAGE and electrospray mass spectroscopy. The protein concentration was determined spectrophotometrically using the average molecular mass and the extinction coefficient E280 = 14 100 M^{-1} cm^{-1}.[36] In our hands, 40 mg of pure uniformly ^{13}C,^{15}N enriched thioredoxin per liter of minimal medium was obtained. Sample preparation for solid-state NMR measurements is described below.

Preparation of Microcrystalline and PEG-Precipitated *E. coli* Thioredoxin. The uniformly ^{13}C,^{15}N enriched thioredoxin sample for the solid-state NMR studies was prepared by controlled precipitation of the protein with poly(ethylene glycol) 4000 (PEG-4000), similar to the procedure described previously.[24] A solution of PEG-4000 containing 10 mM $NaCH_3COO$ and 1 mM NaN_3 (pH 3.5) was slowly added to the solution containing 70 mg/mL of thioredoxin in 10 mM phosphate buffer (pH 7.0), until no further protein precipitation was observed; the final concentration of PEG-4000 was estimated to be 30−35%. Nearly complete precipitation with yields better than 95% was achieved after 24 h, as estimated by the residual absorbance of the supernatant at 280 nm. The hydrated PEG precipitate was centrifuged, and transferred after the supernatant removal into a 4 mm Bruker HRMAS rotor assembly. The samples were sealed using the upper spacer and the top spinner, according to the standard procedures. The natural abundance thioredoxin samples were transferred into a 4 mm Doty or a 4 mm Varian/Chemagnetics rotor following the same procedure.

TABLE 1: Medium- and Long-Range $^{13}C-^{13}C$ Correlations Observed in DARR Spectra Acquired with Mixing Times of 100 and 200 ms

residues	distance, Å	type of correlation
I23Cδ1-T54Cγ2	3.95	long-range: interstrand
L79Cδ1-T89Cβ	4.07	long-range: interstrand
I23Cδ1-A56Cβ	4.14	long-range: interstrand
I23Cδ1-T54Cβ	4.2	long-range: interstrand
I60Cγ2-A67Cβ	4.22	long-range: interstrand
I38Cβ-I41Cδ1	4.5	medium-range: intrahelix $i-(i+3)$
G65Cα-P68Cδ	4.54	medium-range: intrahelix $i-(i+3)$
I41Cδ1-K96Cα	4.54	long-range: interstrand
I72Cγ1-T77Cβ	4.58	long-range: loop termini
I23Cα-T54Cα	4.63	long-range: interstrand
I4Cδ1-D43Cα	4.64	long-range: helix-strand
L79Cγ-T89Cβ	4.72	long-range: interstrand
L79Cβ-T89Cγ2	4.72	long-range: interstrand
L79Cα-T89Cβ	4.73	long-range: interstrand
P34Cα-M37Cϵ	4.76	medium-range: intrahelix $i-(i+3)$
I72Cγ2-T77Cγ2	4.77	long-range: loop termini
I72Cγ2-G74Cα	4.84	medium-range: intraloop $i-(i+2)$
P34Cα-M37Cα	4.87	medium-range: intrahelix $i-(i+3)$
A67Cβ-I72Cα	5.11	long-range: interhelix
A67Cα-I72Cα	5.25	long-range: interhelix
I41Cγ2-I45Cδ1	5.26	medium-range: intrahelix $i-(i+4)$
I23Cδ1-T54Cα	5.26	long-range: interstrand
G33Cα-C35Cα	5.31	Medium-range: intrahelix $i-(i+2)$
L79Cβ-T89Cβ	5.31	Long-range: interstrand
C35Cα-M37Cα	5.38	Medium-range: intrahelix $i-(i+2)$
I38Cδ1-P76Cδ	5.42	long-range: helix-to-strand
T66Cβ-P68Cδ	5.59	medium-range: intrahelix $i-(i+2)$
I45Cδ1-K96Cα	5.65	long-range: interhelix
I60Cγ2-I72Cγ2	5.97	long-range: interstrand
P34Cβ-I38Cγ2	6.12	medium-range: intrahelix $i-(i+4)$
G74Co-P76Cβ	6.46	medium-range: intraloop $i-(i+2)$
G65Cα-A67Cβ	6.52	medium-range: intrahelix $i-(i+2)$
T54Cβ-A56Cα	6.54	medium-range: intrastrand $i-(i+2)$

Solid-State NMR Spectroscopy. Solid-state NMR spectra were acquired at 17.6 T on a wide-bore Bruker Avance spectrometer operating at Larmor frequencies of 750.22 MHz for ^1H, 188.64 MHz for ^{13}C, and 76.02 MHz for ^{15}N. A double-resonance 4 mm HX probe was employed for the homonuclear experiments; the heteronuclear correlations were performed using a triple-resonance 4 mm narrow bore HCN probe. Spectra were recorded using 10 mg of the uniformly ^{13}C,^{15}N enriched thioredoxin sample. The MAS frequency was 10 kHz, and was controlled to within ±1 Hz by a Bruker MAS controller. The actual sample temperature was −15 °C (calibrated using $PbNO_3$ as the temperature sensor[37−39]) and was controlled to within ±0.5 °C throughout the experiments. ^{13}C chemical shifts were referenced with respect to adamantane used as an external standard, where the chemical shift of its more deshielded carbon was assumed to be 38.6 ppm; 1.7 ppm was subsequently added, to adjust the reference scale to 2,2-dimethylsilapentane-5-sulfonic acid DSS.[40] ^{15}N chemical shifts were indirectly referenced with respect to solid NH_4Cl (39.2 ppm with respect to liquid ammonia at 25 °C).[41] This referencing procedure yields chemical shifts which are in close agreement (within the measurement error imposed by the ^{13}C and ^{15}N linewidths) with the IUPAC recommendations for chemical shift referencing in protein spectra.[42] Table 1 of the Supporting Information

summarizes the experimental solid-state chemical shifts in thioredoxin obtained by assigning the backbone and sidechain resonances, as will be described in more detail below.

In Figure 1, the pulse sequences are shown for two-dimensional experiments used for intraresidue and sequential assignments. Five experiments were conducted: NCO (for sequential backbone correlations), NCA (for intraresidue backbone correlations), CXCY (for intraresidue and sequential sidechain correlations), NCACB (for intraresidue backbone/sidechain correlations), and NCOCX (for sequential backbone/sidechain correlations).

The two-dimensional $^{13}C-^{13}C$ chemical shift correlation spectra were acquired using a rotary-assisted proton driven spin diffusion experiment (RAD, DARR) at $N = 1$.[43] During the initial 1.5 ms cross-polarization period, the ^1H amplitude was linearly ramped from 80% to 100%, with the center of the ramp corresponding to the 1st Hartmann−Hahn spinning sideband. During the ^{13}C chemical shift evolution period in the indirect dimension, CW heteronuclear $^1H-^{13}C$ decoupling was used. Throughout the DARR mixing and detection, the 70 kHz XiX decoupling was applied.[44] Four sets of spectra were acquired using DARR mixing times of 2, 10, 100, and 200 ms. The spectral widths for these two data sets were 50 kHz in both dimensions, and the ^{13}C frequency was centered at 95 ppm. Thirty two scans were added for the final FIDs in each t_1 transient. A total of 400 t_1 transients were acquired; recycle delays of 2 s were employed. The total acquisition time was 7.1 h. The following field strengths were used for ^1H excitation: 125 kHz for hard pulses, 58 kHz (corresponding to the center of the ramp) for cross polarization, 70 kHz during decoupling. Irradiation (10 kHz) was applied to ^1H during the mixing period. On the ^{13}C channel, the following field strengths were employed: 48 kHz for cross polarization, and 53.5 kHz for $\pi/2$ and π pulses during the mixing period, respectively. Additional DARR data sets were acquired at 14.1 T, under the same experimental conditions.

Two-dimensional $^{15}N-^{13}C$ correlation spectra were acquired using a SPECIFIC-CP mixing sequence[45] to establish either the N−Cα or the N−Co correlations. During the initial 3 ms cross-polarization period, the ^1H amplitude was linearly ramped from 80% to 100%, with the center of the ramp corresponding to $\omega_1(^1H) = 35$ kHz and $\omega_1(^{15}N) = 28$ kHz. During the ^{15}N chemical shift evolution period in f_1, CW heteronuclear $^1H-^{15}N$ decoupling was used. The polarization was subsequently transferred from the amide nitrogen atoms to either Cα (in the NCA experiment) or Co (in the NCO experiment) carbons via a selective double cross polarization, with the ^{15}N amplitude being linearly ramped from 80% to 100%. The cross-polarization mixing time was 6 ms; $\omega_1(^{15}N) = 25$ kHz (center of the ramp) and $\omega_1(^{13}C) = 18$ kHz. Due to the probe restrictions on the maximum amount of power, the heteronuclear decoupling field strength was kept at 50 kHz throughout the experiment, and the XiX decoupling scheme was employed. The ^{15}N frequency was centered at 119 ppm; the ^{13}C frequency was centered at 51 ppm (in the NCA experiment) or at 180 ppm (in the NCO experiment). A total of 208 (NCO) or 224 (NCA) scans were added for the final FIDs in each t_1 transient; a total of 185 t_1 transients were acquired; recycle delays of 3 s were employed. The total experiment times were 32 and 34 h for the NCO and NCA experiments, respectively.

In the NCACB experiment, the backbone amide nitrogens were correlated with the C_α and the C_β resonances incorporating an additional mixing period with a band-selective DREAM mixing sequence.[20,46] The double-quantum matching condition

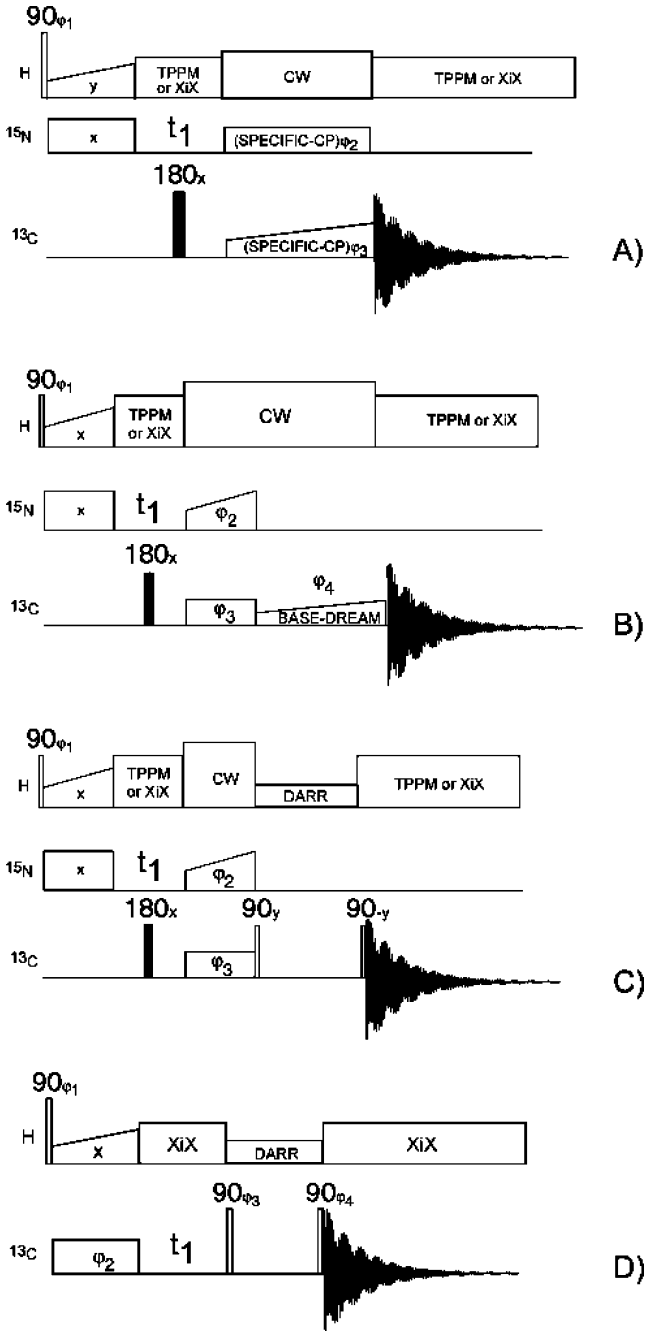

Figure 1. Pulse sequences for two-dimensional NCA/NCO (A), NCACB (B), NCOCX (C), and DARR (D) experiments used in the backbone assignments of thioredoxin. Open rectangles represent $\pi/2$ pulses; filled rectangles represent π pulses. (A) SPECIFIC-CP with a mixing time of 8 ms was utilized for the N-Cα(Co) transfers. The phase cycle was the following: $\varphi_1 = xx\bar{x}\bar{x}$; $\varphi_2 = x\bar{x}x\bar{x}$; $\varphi_3 = (x)_4(y)_4$; $\varphi_{rec} = x\bar{x}\bar{x}xy\bar{y}\bar{y}y$. (B) Band-selective double-quantum DREAM mixing sequence (BASE-DREAM) with a mixing time of 2 ms was employed to selectively transfer magnetization from C_α to C_β carbons in the NCACB experiment. The phase cycle was the following: $\varphi_1 = yy\bar{y}\bar{y}$; $\varphi_2 = x\bar{x}x\bar{x}x\bar{x}x$; $\varphi_3 = (x)_4(\bar{x})_4$; $\varphi_4 = (x)_4(\bar{x})_4$; $\varphi_{rec} = x\bar{x}\bar{x}x$. (C) DARR mixing (10 ms mixing time) was used to record the NCOCX spectra. The phase cycle was the following: $\varphi_1 = yy\bar{y}\bar{y}$; $\varphi_2 = x\bar{x}x\bar{x}x\bar{x}x$; $\varphi_3 = (x)_4(\bar{x})_4$; $\varphi_{rec} = x\bar{x}\bar{x}x$. (D) DARR experiments with mixing times of 2 and 10 ms were used to establish the one- and some two-bond correlations. A DARR mixing time of 100 ms was employed to yield medium-range correlations. The phase cycle was the following: $\varphi_1 = y\bar{y}$; $\varphi_2 = xx\bar{x}\bar{x}$; $\varphi_3 = (y)_4(\bar{y})_4$; $\varphi_4 = (x)_8(\bar{x})_8$; $\varphi_{rec} = x\bar{x}\bar{x}x(\bar{x}x\bar{x}x)_2x\bar{x}\bar{x}x$.

$n\omega_r = (\omega_{rf}^2 + \Omega_1^2)^{1/2} + (\omega_{rf}^2 + \Omega_2^2)^{1/2}$ in conjunction with the chemical shift difference for the $C_\alpha-C_\beta$ pair ($\Delta\Omega = 20-40$

ppm) dictates the experimental setup, which for 17.6 T involves an rf field ramp of ca. 3−6 kHz for $n = 1$, and the spectrometer frequency centered around 40 ppm. For the NCOCX experiment, DARR[43] C−C mixing followed the first N−Cα/N−Co transfer step, correlating the backbone amide resonances with the sidechain carbons. In each experiment, 224 scans were added for the final FIDs in each t_1 transient; a total of 190 t_1 transients were acquired; recycle delays of 2 s were employed. The total experiment time was 23.6 h.

Additionally, one-dimensional ^{13}C CPMAS spectra were recorded at 9.4, 14.1, and 17.6 T, with a spinning frequency of 10 kHz. The ^{1}H amplitude was linearly ramped from 80% to 100%, with the center of the ramp corresponding to $\omega_1(^1H) = 59$ kHz; $\omega_1(^{15}N)$ (or $\omega_1(^{13}C)) = 49$ kHz. XiX decoupling at a field strength of 70 kHz was applied during the acquisition. A total of 128 or 512 scans were added to form the final FIDs in the ^{15}N or ^{13}C spectra, respectively; the acquisition time was 50 ms.

The data were processed in NMRPipe[47] under the Linux environment on a Dell Precision workstation. The NCA, NCO, NCACB, NCACX, NCOCX, and CC spectra were processed with Gaussian apodization in both dimensions, zero filling up to 4096 points in f_2 and 512 points in f_1. Additionally, the CC, NCACB, NCACX, and NCOCX spectra were processed with resolution enhancement, by applying a 60° shifted sine apodization in f_2, and 30° shifted sine apodization in f_1. The spectral assignments were performed in Sparky.[48] The statistical analysis of the secondary shifts and prediction of backbone dihedral angles were performed in TALOS.[49]

Results and Discussion

Sample Conditions for Solid-State NMR Experiments. For all solid-state NMR measurements discussed in this work, the thioredoxin samples were prepared from poly(ethylene glycol) (PEG) solutions, following the controlled precipitation procedure. Similar to our work on reassembled thioredoxin reported recently,[24] high-quality spectra were obtained for the full-length thioredoxin via this procedure, and permitting the majority of the resonances to be readily assigned, as discussed below. The ^{13}C and ^{15}N linewidths for the outlying peaks in the CPMAS spectra are 40−100 and 20−40 Hz, respectively. These line widths are field independent as illustrated in Figure 2, for the data sets acquired at 17.6 and 14.1 T.

Compared with the micro- and nanocrystalline preparations,[20,23,50,51] this protocol requires only a minimal screening of precipitation conditions, and the nearly quantitative precipitation with yields of ca. 95−99% is accomplished in less than 24 h. In contrast to micro- and nanocrystalline preparations where the pH is kept close to the isoelectric point of the protein pI, the controlled PEG precipitation can be conducted in a fairly broad range of pH values. For thioredoxin, the maximum yields of the precipitate were obtained at pH values away from the PI. We anticipate that the controlled precipitation procedure could be potentially applicable to a broad range of proteins and protein complexes. Moreover, prior studies indicate that PEG-precipitated proteins are functionally competent.[52,53]

Experimental Protocols and General Considerations for Resonance Assignments of *E. coli* Thioredoxin. Several different assignment protocols have been reported recently.[17,20,21,23,24] As was demonstrated in our study on reassembled thioredoxin, the NCO, NCA, NN, and CXCY correlations were sufficient for the resonance assignments of the overwhelming majority of the residues. Due to the signal overlap in the NCA/NCO spectra of the full-length protein, two additional 2D correlation experiments were necessary: NCACB and NCOCX. The approach employed in this study takes advantage of high magnetic fields yielding nearly complete resonance assignments with a limited number of two-dimensional experiments and with modest amounts of experimental time, even for a protein with the size of thioredoxin. For proteins smaller than thioredoxin, partial backbone resonance assignments can be performed at lower field strengths (7.0 and 9.4 T).[15,16] However, three-dimensional experiments and a field strength of at least 9.4 T are required for nearly complete assignments.[17] Higher magnetic fields appear to be necessary for adequate resolution in the homonuclear $^{13}C-^{13}C$ experiments: as was demonstrated in our previous work on bpti[20] and in this study (Figure 1 of the Supporting Information), at lower magnetic fields the resolution is significantly compromised. Sensitivity is an additional important factor. At 17.6 T (750 MHz), 0.1−0.5 μmol of protein are sufficient for the measurements, and the experimental time ranges between 8 and 30 h. Larger amounts of sample and significantly longer experiment times are necessary at lower fields. For instance, for thioredoxin we observed an ca. 40% reduction in the S/N ratio of the ^{13}C CPMAS spectra at 14.1 T acquired under similar experimental conditions (Figure 2). This reduction in the S/N ratio is consistent with the theoretically expected S/N dependence on the inherent magnetic field strength: $S/N \propto (B_0)^{3/2}$.

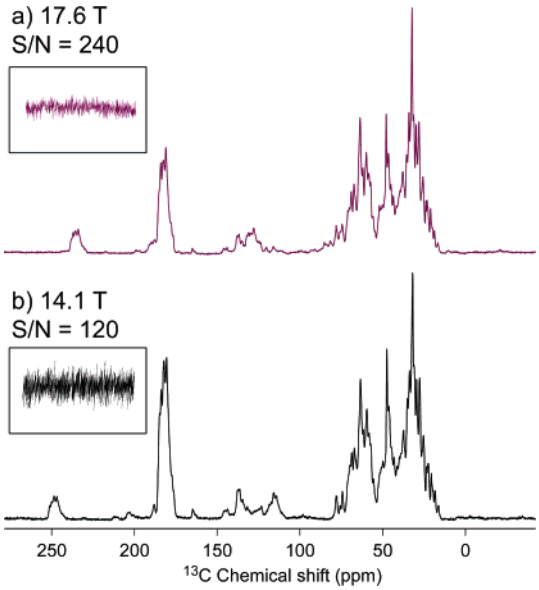

Figure 2. ^{13}C CPMAS spectra of uniformly $^{13}C,^{15}N$-enriched *E. coli* thioredoxin acquired at 17.6 and 14.1 T (a and b, respectively). The 17.6 and 14.1 T spectra were obtained using 10 and 8 mg of protein, respectively. The insets illustrate the noise level in the spectra, plotted to the same scale. The S/N ratio is lower by a factor of 2 in the 14.1 T spectra, amounting to ca. 40% reduction of the S/N ratio due to the lower field alone.

Resonance Assignments. For the intraresidue and the sequential backbone assignments, we utilized the NCA, NCO, NCACB, NCACX, and NCOCX experiments. The sidechain assignments of ^{13}C resonances were based on the DARR spectra acquired with three mixing times: 2, 10, and 100 ms. At a mixing time of 2 ms, predominantly one-bond correlations were observed. At a mixing time of 10 ms, two-bond correlations emerge, and at 100 ms and longer, a number of multibond correlations are present. These corresponded to the medium-range $^{13}C-^{13}C$ distances, and were useful for confirming sequential assignments. The pulse sequences for the individual experiments are illustrated in Figure 1. The experimental spectra

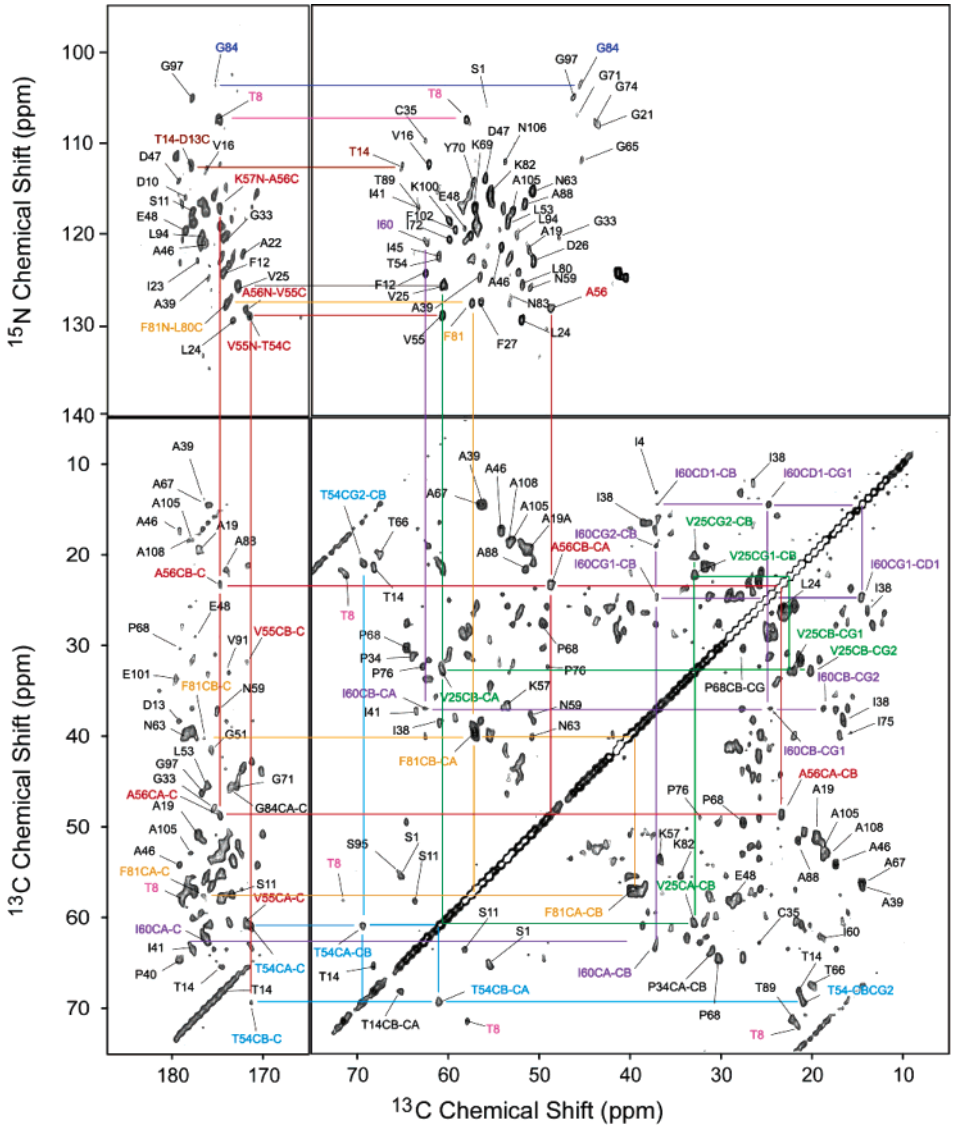

Figure 3. CXCY (A), NCO (B), and NCA (C) spectra of *E. coli* thioredoxin demonstrating examples of intraresidue and sequential backbone and sidechain assignment walks. The CXCY spectrum was recorded with the DARR mixing element and a mixing time of 10 ms resulting in predominantly one-bond correlations, and a limited number of two-bond intraresidue correlations. The spectra were processed with Gaussian apodization in both dimensions, zero filling up to 4096 points in the direct dimension, and 512 points in the indirect dimension.

employed in the backbone and sidechain assignments are shown in Figures 3−6. In Figures 5 and 6, examples of sequential cross-peaks present in the DARR experiment (100 ms mixing time) are illustrated. Additionally, several medium- and long-range correlations are displayed in Figure 6.

The starting point of the process was the identification of the amino acid sidechain ^{13}C spin topologies from the DARR spectrum acquired with a mixing time of 2 ms. For example, the three serines, nine glycines, five of the six threonines, and a large number of prolines, isoleucines, leucines, valines, lysines, and alanines were readily identified based on their characteristic resonances in the isolated regions of the spectrum, and on the one-bond correlation patterns. These assignments were further confirmed by the intraresidue two- and three-bond correlations present in the DARR spectra recorded with a mixing time of 10 ms. The intraresidue backbone correlations were established in the NCA and NCACB experiments.

Sequential connectivities were derived from the NCO, NCOCX, and DARR (100 ms) experiments. The NCO experiment was employed for identification of a large number of the backbone carbonyl carbons from the correlations between the amide nitrogen of a particular residue and its sequential ($i - 1$) carbonyl carbon. Most of these assignments were further corroborated by the DARR experiments acquired with mixing times of 2 and 10 ms. The aliphatic region of the NCOCX spectra was particularly useful for unambiguous assignments of the sidechain resonances of residues exhibiting a high degree of overlap in the DARR spectra, i.e., leucines, lysines, and valines. These were determined via multiple sequential correlations between the sidechain carbons and the amide nitrogens of the succeeding residue. Additionally, the carbonyl region of the spectrum was useful in resolving the Cγ and Cδ resonances of asparagines, aspartic, and glutamic acids.

Following this approach, we were able to site-specifically assign 107 of the 108 residues in thioredoxin, with the exception of A29. The assignment of this residue was not feasible because of the overlap with the resonances belonging to other alanines. Furthermore, these ambiguities could not be resolved by detecting the expected sequential correlations with the Cα and Cβ resonances of W28 in the DARR spectra with long mixing times, or by the correlations with the amide nitrogen of E30 in the NCOCX experiment, due to the poor dispersion in that region. Below, site-specific assignments of several residue types are discussed.

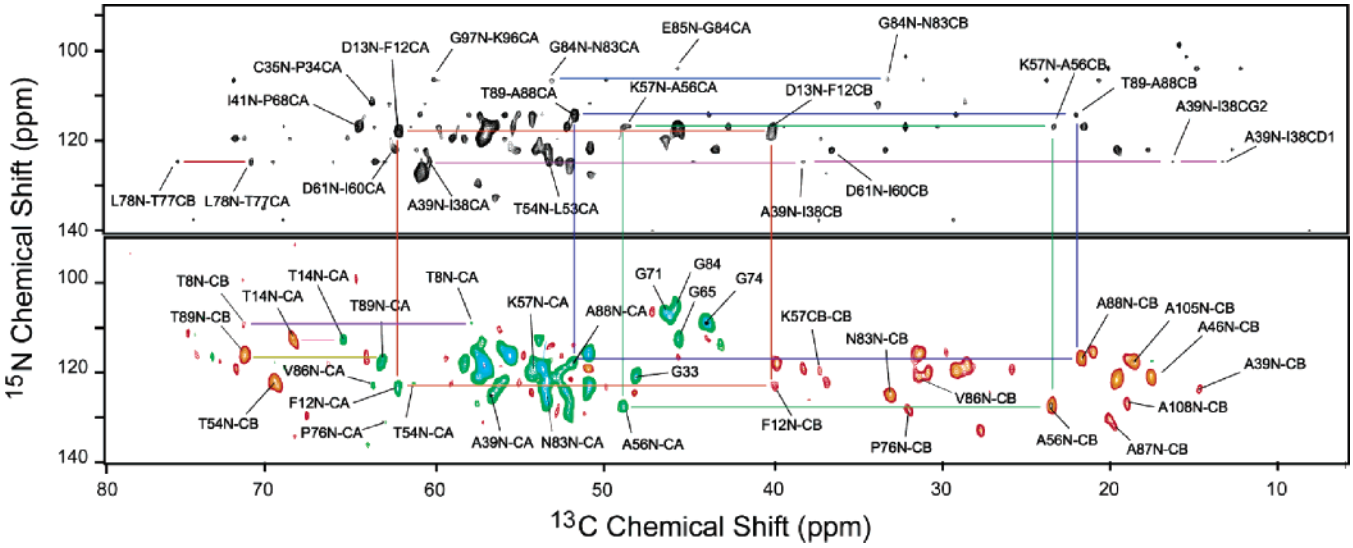

Figure 4. NCACX (top) and NCACB (bottom) spectra of *E. coli* thioredoxin. Examples of intraresidue ^{15}N−^{13}Cα−^{13}Cβ correlations are shown for selected residues. The SPECIFIC-CP sequence was used to establish the first ^{15}N−^{13}C transfer, followed by an additional mixing period with either the DARR (for NCACX) or the band-selective DREAM (for NCACB) mixing sequences.

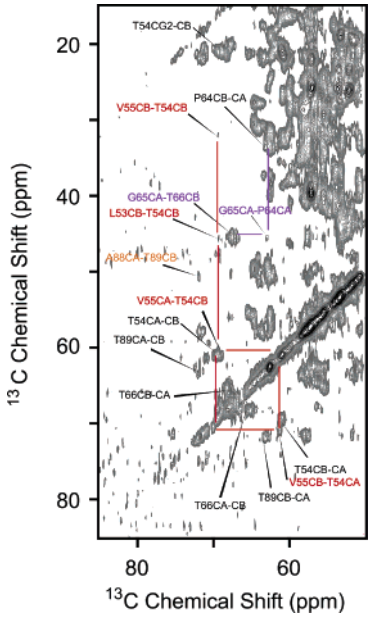

Figure 5. Expansions of the 100 ms CXCY DARR spectrum, demonstrating examples of sequential cross-peaks.

Serines were used as the starting point in the assignment process due to their low occurrence in the sequence (only three are present: S1, S11, and S95), their characteristic deshielded Cβ resonance at ca. 64 ppm, and the excellent resolution of their aliphatic region in the DARR spectra. S95 could be unambiguously assigned via the multiple sequential correlations observed in the NCOCX spectrum, e.g., S95N-L94Cα, S95N-L94Cβ, S95N-L94Cγ, S95N-L94Cδ2, K96N-S95Cα, and K96N-S95Cβ. Additional sequential cross-peaks were present in the DARR experiment acquired with a mixing time of 100 ms (e.g., S95Cα-K96Cα and K96Cβ-S95Cα), and in the NCO spectrum (e.g., S95N-L94Co and K96N-S95Co). Similarly, identification of S11 relied on the sequential correlations with D10 and F12 present in the NCOCX and NCO spectra: S11N-D10Cα, S11N-D10Cβ; F12N-S11Cα, F12N-S11Cβ; and S11N-D10Co, F12N-S11Co. Additional intraresidue correlations observed in the NCACB experiment corroborated the identities of the α and the β carbons. S1 was assigned based on the sequential cross-peaks in an isolated region of the DARR spectrum recorded with a mixing time of 100 ms, i.e., S1Cβ-D2Cα and S1Cβ-D2Cβ.

Identification of the six threonines, T8, T14, T54, T66, T77, and T89, was based on their typical downfield Cβ chemical shift (ca. 70 ppm), and their characteristic CC intraresidue correlations in the DARR spectra. Site-specific assignments of each threonine were based on multiple sequential correlations observed in the NCOCX, NCO, and DARR (100 ms) experiments. For example, T89, located between A88 and K90, was identified from the NCOCX, NCO, and DARR (100 ms) correlations, e.g., T89N-A88Cα, T89N-A88Cβ, K90N-T89Cα, K90N-T89Cβ and K90N-T89Cγ2, K90N-T89Co, and A88Cα-T89Cβ. Additional long-range correlations with L79 also confirmed the assignment of T89: T89Cβ-L79Cδ1, T89Cβ-L79Cγ, T89Cβ-L79Cβ, and T89Cβ-L79Cα. These long-range correlations also provide useful tertiary constraints, as discussed in more detail in the corresponding section of this report.

Thioredoxin has nine glycine residues: G21, G33, G51, G65, G71, G74, G84, G92, and G97. These were readily identified in the NCA and NCACB spectra by their characteristic upfield Cα chemical shifts and by the Cα-Co correlations present in the DARR (2 ms) experiment. Site-specific assignment was accomplished by the multiple sequential correlations with their neighboring residues, observed in the NCOCX, NCO, and DARR (100 ms) experiments. For example, G33, located between C32 and P34, was site-specifically assigned by NCO and NCOCX correlations (e.g., G33N-C32Cα, G33N-C32Cβ, G33N-C32Co, and P34N-G33Co). Additionally, a large number of sequential and medium-range DARR correlations were useful for corroborating this assignment (e.g., P34Cα-G33Cα, P34Cβ-G33Cα, P34Cδ-G33Cα, and G33Cα-C35Cα).

Identification of the aromatic residues was based on the one-bond correlations between the aromatic and the aliphatic carbons as well as on their typical aromatic carbon chemical shifts. For example, the Cγ's of the tryptophan residues are usually most shielded among the aromatics (with shifts of ca. 108 ppm), whereas the Cζ's of arginines typically appear at the other extreme (of ca. 160 ppm). Identification of the two tryptophans, W28 and W31, was based on their multiple aromatic−aliphatic cross-peaks in the DARR spectrum acquired with a mixing time of 10 ms, e.g., W31Cβ-Cγ, W31Cβ-Cδ1, W31Cβ-Cδ2, W31Cβ-Cϵ2, W28Cα-Cγ, W28Cβ-Cγ, W28Cγ-Cδ, and W28Cγ-Cδ2.

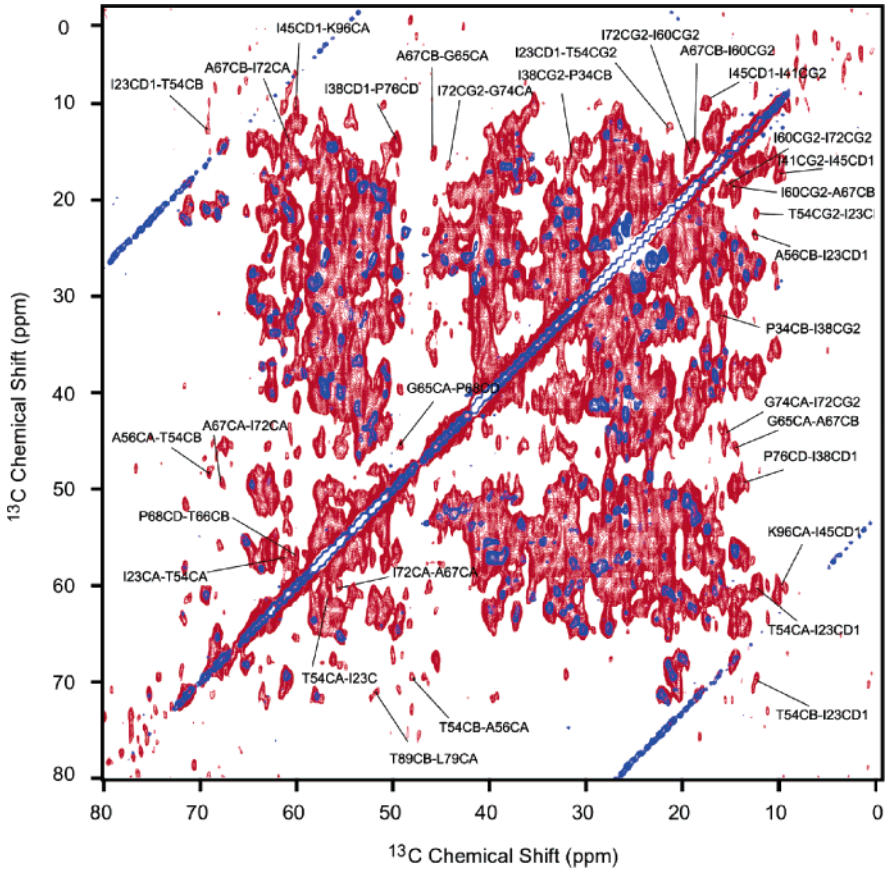

Figure 6. Overlay of CXCY DARR spectra of full length *E. coli* thioredoxin acquired with mixing times of 2 and 200 ms (blue and red spectra, respectively). Examples of medium- and long-range $^{13}C-^{13}C$ correlations are demonstrated. The spectra were processed using a cosine filter in both dimensions, zero filling to 4096 points in the f_2 dimension and 1024 points in the f_1 dimension, and automatic baseline correction in the f_2 dimension.

Site-specific assignments relied on the sequential correlations present in the NCOCX and NCO experiments, e.g., W31N-E30Cα, W31N-E30Cβ, W31N-E30Cγ, W31N-E30Cδ, C32N-W31Cα, C32N-W31Cβ, W31N-E30Co, and C32N-W31Co.

Identification of the 11 (of 12) alanines, A19, A22, A46, A39, A56, A67, A87, A88, A93, A105, and A108, was accomplished based on the multiple sequential correlations present in the NCOCX, NCO, and DARR (100 ms) experiments, as well as from the typical CC intraresidue correlations observed in the DARR (2 and 10 ms) spectra. For example, A39 and A67 were difficult to assign due to their similar ^{13}C shifts in the aliphatic regions of the spectra. However, the cross-peaks between A39 and A67 and their neighboring residues observed in the NCOCX and DARR (100 ms) experiments were essential for distinguishing between these two residues. For example, the following cross-peaks of A39 with I38 and P40 were identified: A39N-I38Cα, A39N-I38Cβ, A39N-I38Cγ1, A39N-I38Cγ2, A39N-I38Cδ1, P40N-A39Cα, and P40N-A39Cβ. For A67, the corresponding correlations included A67N-T66Cα, A67N-T66Cβ, A67N-T66Cγ2, and P68N-A67Cα. Additional correlations present in the DARR spectrum acquired with a mixing time of 100 ms corroborated the identity of these two alanines: I38Cα-A39Cβ, I38Cβ-A39Cβ, P40Cα-A39Cβ, P40Cβ-A39Cβ, P40Cδ-A39Cβ, A67Cβ-P68Cα, A67Cβ-P68Cβ, A67Cβ-T66Cβ, A67Cβ-P68Cδ, and P68Cα-A67Cβ.

A similar approach was employed for the unambiguous assignments of other residues in the sequence (see the Supporting Information for additional details). In summary, we were able to site-specifically assign 98% of the backbone ^{13}C and ^{15}N chemical shifts, and 90% of the sidechain ^{13}C resonances of the *E. coli* thioredoxin, by a combination of 2D homo- and heteronuclear correlation experiments. These chemical shifts are summarized in Table 1 of the Supporting Information.

Backbone Dihedral Angles and Secondary Structure Analysis. Secondary carbon and nitrogen chemical shifts are sensitive indicators of the polypeptide backbone conformation.[54] Empirical predictions of the dihedral ψ and ϕ angles based on the statistical analysis of the secondary chemical shifts have been implemented in TALOS,[49] and widely applied in solution NMR for deriving protein secondary structure. Recently, the same approach was demonstrated to yield accurate results for the solid-state chemical shifts of several peptides and proteins.[23,24,55,56]

In Figure 7, the dihedral angles derived from the secondary solid-state chemical shifts are depicted and compared with the corresponding values predicted from solution shifts. The overwhelming majority of ψ angles (99° of 108°) and of ϕ angles (103° of 108°) deviate by less than 25° in the solid state vs. solution, with mean values of 13° and 14° for ψ and ϕ, respectively. The largest deviations are observed for S11, D20, Q62, R73, and G74. With the exception of Q62, these discrepancies are not surprising, since all of these residues are located either in the loop regions connecting the main secondary elements or at the termini of the β-sheets or α-helices. Q62 is located in the middle of a short 5-residue α-helix and is solvent exposed, which may possibly account for the observed differences. These results are illustrated in Figure 8.

Additionally, we have compared the dihedral angles derived in this study with those reported recently for the 35-residue C-terminal fragment of the *E. coli* reassembled thioredoxin.[24] The results are summarized in Figure 1 of the Supporting Information. As anticipated, the dihedral angles are in good

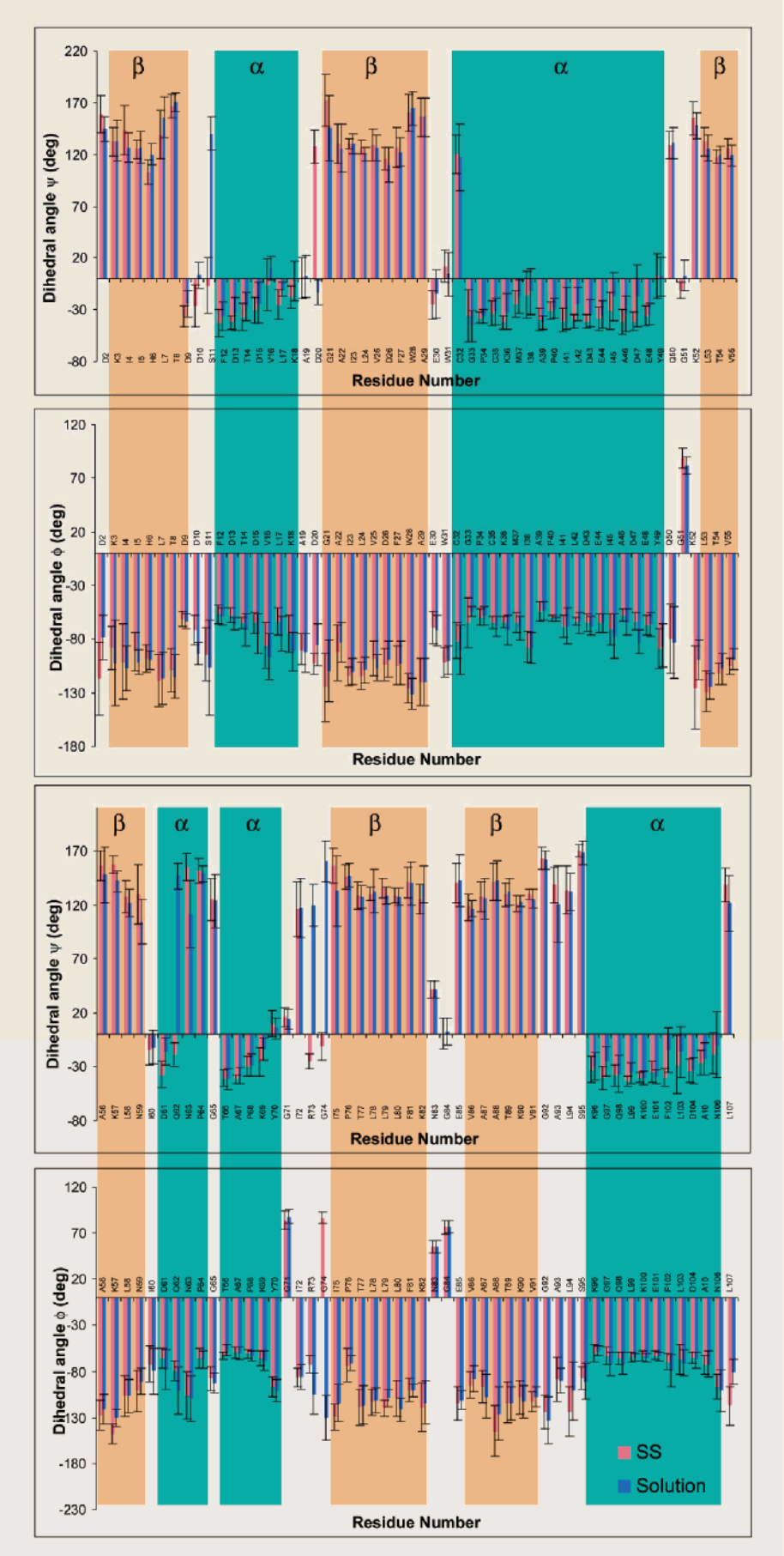

Figure 7. Comparison of the dihedral ψ angles predicted from the observed solid-state and solution chemical shifts of *E. coli* thioredoxin, using TALOS.[49] The red and blue rectangles represent solid-state and solution values, respectively. The α-helical and β-sheet regions in the secondary structure are highlighted.

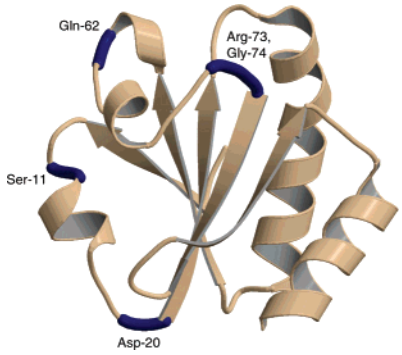

Figure 8. Thioredoxin structure representation based on the PDB file (2trx), generated in Molscript[61] and Raster3D.[62,63] Residues whose dihedral angles predicted from solid-state and solution NMR chemical shifts differ by more than 25° are highlighted in dark blue. These residues are located in the termini of the individual α-helices, β-sheets, or flexible loops.

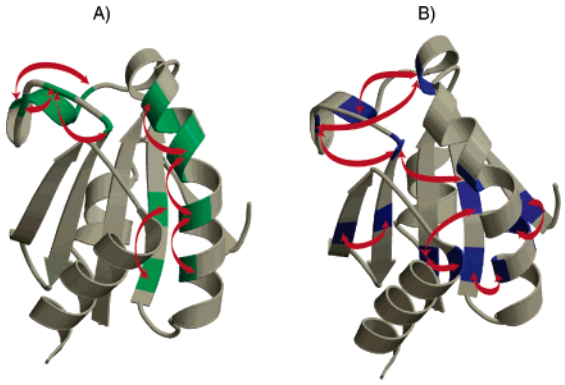

Figure 9. Thioredoxin structure representation based on the PDB file (2trx), generated in Molscript[61] and Raster3D,[62,63] and depicting (A) medium-range and (B) long-range correlations unambiguously assigned from DARR spectra obtained with mixing times of 100−200 ms. The corresponding residues are color coded green and blue, respectively, and arrows illustrate examples of the observed correlations.

agreement for the majority of the residues, with the exception of N83, A87, and N106. N83 and N106 are located in a loop region and in the C-terminus; therefore, the disagreement is not surprising. For A87 in the full-length thioredoxin described in this work, the predicted dihedral angles are in agreement with both solution NMR and X-ray crystallography results, and correspond to the location of this residue in a β-sheet. As was discussed in our recent report,[24] the reason for the disagreement between the dihedral angles for A87 in the reassembled thioredoxin predicted from solid-state shifts and those derived from solution NMR and X-ray crystallography measurements is not clear, and further measurements would be required to address this inconsistency.

In summary, the secondary structure of *E. coli* thioredoxin is correctly derived from solid-state NMR data, providing additional evidence to the general applicability of the TALOS prediction algorithm to solid-state NMR chemical shifts.

Analysis of Medium- and Long-Range Correlations in the Homonuclear ^{13}C Correlation Spectra. DARR spectra with mixing times in the range of 100−200 ms contain multiple weak yet well-resolved cross-peaks, corresponding to medium- and long-range correlations, as illustrated in Figure 6. Due to the large number of resonances, the complete unambiguous assignment of these cross-peaks based on the 2D DARR spectra alone was not feasible. However, we have identified and assigned a number of medium- and long-range cross-peaks appearing in isolated regions of the spectra, and corresponding to the following residues: I4, I23, P34, C35, M37, I38, I41, D43, I45, T54, A56, I60, G65, T66, A67, P68, I72, G74, P76, T77, L79, T89, and L79. The results are summarized in Table 1 and Figure 9. For these residues, at least two medium- or long-range correlations per pair were observed, corresponding to distances ranging between ca. 3.9 and 6.5 Å. Correlations I4-D43, L79-T89, A67-I72, and I72-T77 correspond to the long-range contacts between the individual secondary structure elements, indicating that the cross-peaks in the DARR spectra with long mixing times could provide meaningful distance restraints in the tertiary structure calculations. Moreover, at mixing times of 100−200 ms the intensities for the medium- and long-range cross-peaks were 5−20% of those for one-bond cross-peaks, indicating that the attenuation of the long-range correlations by dipolar truncation is not as severe as observed previously for other recoupling sequences.[57,58] Our findings are in agreement with the recent reports by Takegoshi, Nakamura, and Terao,[59] as well as by Smith and collegues,[60] concluding that dipolar truncation does not impede observation of long-range correlations in DARR spectra. These results suggest that DARR experiments with uniformly enriched proteins might present an efficient approach for gaining tertiary restraints for protein structure determination by solid-state NMR.

To understand the polarization transfer dynamics in DARR experiments, we compared the DARR buildup curves corresponding to the one-bond and long-range correlations (illustrated in Figure 10). As expected, the one-bond correlations build up quickly, within the first 10 ms, and subsequently decay with a time constant of several hundred milliseconds. In contrast, the long-range correlations build up much slower, within 100−200 ms. Note that at a mixing time of 200 ms the one-bond cross-peaks decayed by a factor of 1.5−2, while the corresponding multibond correlations are at their maximum intensity. These buildup curves suggest an additional possible reason for the seemingly high multibond cross-peak relative intensities in the DARR spectra acquired with long mixing times.

Despite the large number of medium- and long-range cross-peaks that could be unambiguously identified in the 2D DARR spectra, many additional cross-peaks that we attributed to long-range correlations could not be assigned, due to the spectral complexity or overlap. It appears that to complete assignments of these long-range cross-peaks, an additional dimension will need to be introduced. Whether a sufficient number of interpretable constraints can be obtained to define the tertiary structure using this approach in uniformly isotopically enriched proteins remains an open question, and is currently under investigation in our laboratory.

Conclusions

Resonance assignments for the uniformly ^{13}C,^{15}N-enriched *E. coli* thioredoxin have been derived from two-dimensional solid-state magic angle spinning spectroscopy at 17.6 T. Statistical analysis of ^{13}C and ^{15}N chemical shifts accurately predicts backbone dihedral angles and secondary structure for the overwhelming majority of amino acid residues in thioredoxin. The analysis of DARR spectra acquired with long mixing times revealed a large number of meaningful medium- and long-range correlations, which could be potentially useful for defining the tertiary structure of thioredoxin based on the solid-state NMR data alone.

The 108 amino acid residue thioredoxin is the largest uniformly enriched protein assigned to date by MAS NMR spectroscopy. The experimental protocols utilized in this work

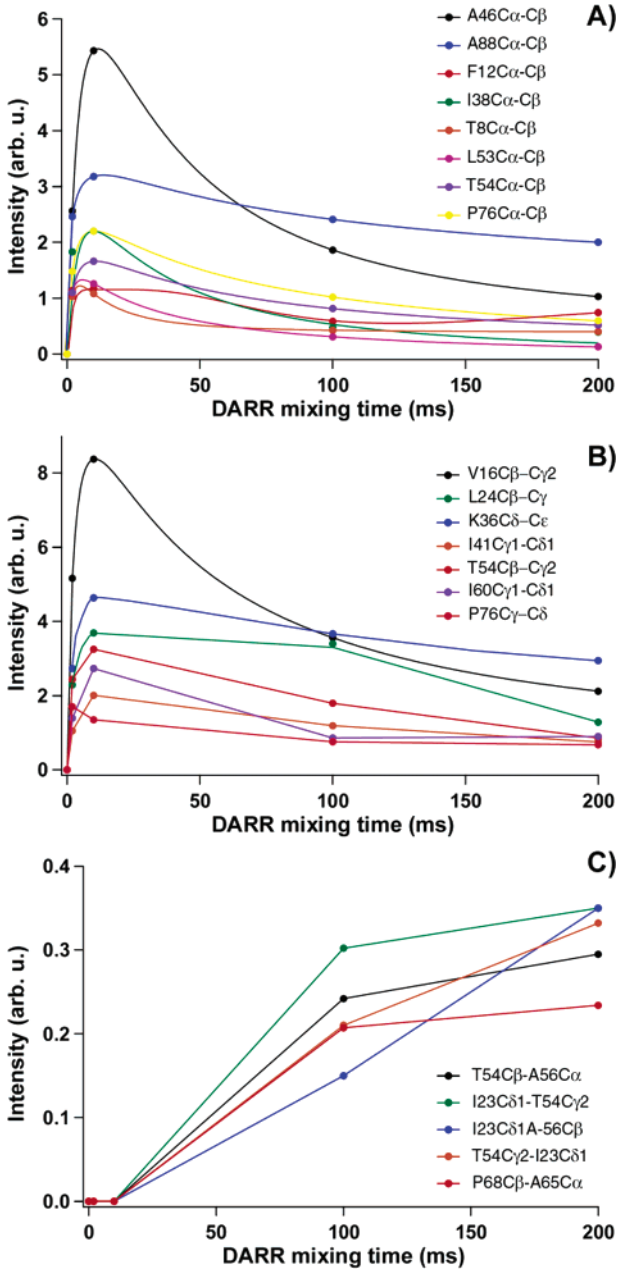

Figure 10. Buildups of selected cross-peak absolute intensity in the DARR spectra of *E. coli* thioredoxin: (a) one-bond Cα−Cβ correlations; (b) one-bond correlations between sidechain carbon atoms; and (c) multiple-bond medium- and long-range correlations. Note that one-bond correlations build up within the first 10 ms and subsequently decay with a time constant of several hundred milliseconds, while the multiple bond correlations reach their maximum intensity after 200 ms. The absolute intensities are plotted using the same scale on the *y*-axis for the three mixing times.

are expected to be generally suited for structural studies of larger proteins by high-resolution solid-state NMR spectroscopy.

Acknowledgment. We gratefully acknowledge Professor Ann McDermott for many valuable discussions. T.P. (as adjunct faculty of CUNY) and M.L.T. are members of the New York Structural Biology Center supported in part by the National Institutes of Health (P41 GM066354) and its Member Institutions, and gratefully acknowledge the instrument time on the 750 MHz solid-state NMR spectrometer at the Center. T.P., M.L.T., and D.M. have been supported by the National Institutes of Health (5S06GM060654-04; SCORE program individual subproject). T.P. acknowledges support of the National Science Foundation CAREER development award (CHE 0350385), of the National Institutes of Health (P20-17716 under COBRE program and 2 P20 016472-04 under INBRE program of NCRR), of the Petroleum Research Fund, administered by the American Chemical Society (PRF grant no. 39827-G5M), and of the University of Delaware. M.L.T. acknowledges support of the National Science Foundation POWRE award (MB 0075115), and of the National Institutes of Health (5G12 RR03060 from the National Center for Research Resources).

Supporting Information Available: Resonance assignments of valine, proline, and glutamate residues, CXCY spectra of full length *E. coli* thioredoxin, and table of ^{15}N and ^{13}C solid-state chemical shifts of *E. coli* thioredoxin. This material is available free of charge via the Internet at http://pubs.acs.org.

References and Notes

(1) Jaroniec, C. P.; Lansing, J. C.; Tounge, B. A.; Belenky, M.; Herzfeld, J.; Griffin, R. G. *J. Am. Chem. Soc.* **2001**, *123* (51), 12929−12930.

(2) Yang, J.; Prorok, M.; Castellino, F. J.; Weliky, D. P. *Biophys. J.* **2004**, *87* (3), 1951−1963.

(3) Henzler-Wildman, K. A.; Martinez, G. V.; Brown, M. F.; Ramamoorthy, A. *Biochemistry* **2004**, *43* (26), 8459−8469.

(4) Buffy, J. J.; McCormick, M. J.; Wi, S.; Waring, A.; Lehrer, R. I.; Hong, M. *Biochemistry* **2004**, *43* (30), 9800−9812.

(5) Isaac, B.; Gallagher, G. J.; Balazs, Y. S.; Thompson, L. K. *Biochemistry* **2002**, *41* (9), 3025−3036.

(6) Watts, A. *Mol. Membr. Biol.* **2002**, *19* (4), 267−275.

(7) Franzin, C. M.; Choi, J. Y.; Zhai, D. Y.; Reed, J. C.; Marassi, F. M. *Magn. Reson. Chem.* **2004**, *42* (2), 172−179.

(8) Thiriot, D. S.; Nevzorov, A. A.; Zagyanskiy, L.; Wu, C. H.; Opella, S. J. *J. Mol. Biol.* **2004**, *341* (3), 869−879.

(9) Nishimura, K.; Kim, S. G.; Zhang, L.; Cross, T. A. *Biochemistry* **2002**, *41* (44), 13170−13177.

(10) Tycko, R. *Prog. Nucl. Magn. Reson. Spectrosc.* **2003**, *42* (1−2), 53−68.

(11) Petkova, A. T.; Buntkowsky, G.; Dyda, F.; Leapman, R. D.; Yau, W. M.; Tycko, R. *J. Mol. Biol.* **2004**, *335* (1), 247−260.

(12) Burkoth, T. S.; Benzinger, T. L. S.; Urban, V.; Morgan, D. M.; Gregory, D. M.; Thiyagarajan, P.; Botto, R. E.; Meredith, S. C.; Lynn, D. G. *J. Am. Chem. Soc.* **2000**, *122* (33), 7883−7889.

(13) Drobny, G. P.; Long, J. R.; Karlsson, T.; Shaw, W.; Popham, J.; Oyler, N.; Bower, P.; Stringer, J.; Gregory, D.; Mehta, M.; Stayton, P. S. *Annu. Rev. Phys. Chem.* **2003**, *54*, 531−571.

(14) Cegelski, L.; Kim, S. J.; Hing, A. W.; Studelska, D. R.; O'Connor, R. D.; Mehta, A. K.; Schaefer, J. *Biochemistry* **2002**, *41* (43), 13053−13058.

(15) Straus, S. K.; Bremi, T.; Ernst, R. R. *J. Biomol. NMR* **1998**, *12* (1), 39−50.

(16) Hong, M. *J. Biomol. NMR* **1999**, *15* (1), 1−14.

(17) Igumenova, T. I.; Wand, A. J.; McDermott, A. E. *J. Am. Chem. Soc.* **2004**, *126* (16), 5323−5331.

(18) Igumenova, T. I. Assignment of uniformly carbon-13-enriched proteins and optimization of their carbon lineshapes. Ph.D. Thesis, Columbia University, New York, 2003.

(19) Igumenova, T. I.; McDermott, A. E.; Zilm, K. W.; Martin, R. W.; Paulson, E. K.; Wand, A. J. *J. Am. Chem. Soc.* **2004**, *126* (21), 6720−6727.

(20) McDermott, A. E.; Polenova, T.; Bockmann, A.; Zilm, K.; Martin, R.; Paulson, E.; Montellione, G. *J. Biomol. NMR* **2000**, *16*, 209−219.

(21) Castellani, F.; van Rossum, B.; Diehl, A.; Schubert, M.; Rehbein, K.; Oschkinat, H. *Nature* **2002**, *420* (6911), 98−102.

(22) Zech, S. G.; Wand, A. J.; McDermott, A. E. *J. Am. Chem. Soc.* **2005**, *127*, 8618−8626.

(23) Bockmann, A.; Lange, A.; Galinier, A.; Luca, S.; Giraud, N.; Juy, M.; Heise, H.; Montserret, R.; Penin, F.; Baldus, M. *J. Biomol. NMR* **2003**, *27* (4), 323−339.

(24) Marulanda, D.; Tasayco, M. L.; McDermott, A.; Cataldi, M.; Arriaran, V.; Polenova, T. *J. Am. Chem. Soc.* **2004**, *126* (50), 16608−16620.

(25) Franks, W. T.; Zhou, D. H.; Wylie, B. J.; Money, B. G.; Graesser, D. T.; Frericks, H. L.; Sahota, G.; Rienstra, C. M. *J. Am. Chem. Soc.* **2005**, in press.

(26) Kiihne, S.; Mehta, M. A.; Stringer, J. A.; Gregory, D. M.; Shiels, J. C.; Drobny, G. P. *J. Phys. Chem. A* **1998**, *102* (13), 2274−2282.

(27) Hodgkinson, P.; Emsley, L. *J. Magn. Reson.* **1999**, *139* (1), 46−59.

(28) LeMaster, D. M.; Kushlan, D. M. *J. Am. Chem. Soc.* **1996**, *118* (39), 9255−9264.
(29) Hong, M.; Jakes, K. *J. Biomol. NMR* **1999**, *14* (1), 71−74.
(30) Etzkorn, M.; Bockmann, A.; Lange, A.; Baldus, M. *J. Am. Chem. Soc.* **2004**, *126* (45), 14746−14751.
(31) Chaffotte, A. F.; Li, J. H.; Georgescu, R. E.; Goldberg, M. E.; Tasayco, M. L. *Biochemistry* **1997**, *36* (51), 16040−8.
(32) Chandrasekhar, K.; Campbell, A. P.; Jeng, M.-F.; Holmgren, A.; Dyson, H. J. *J. Biomol. NMR* **1994**, *4*, 411−432.
(33) Sambrook, J.; Fritsch, E. F.; Maniatis, T. *Molecular Cloning*: *A Laboratory Manual*; Cold Spring Harbor Laboratory Press: Cold Spring Harbor, NY, 1989; Vol. 3, p.
(34) Marley, J.; Lu, M.; Bracken, C. *J. Biomol. NMR* **2001**, *20* (1), 71−75.
(35) Langsetmo, K.; Fuchs, J.; Woodward, C. *Biochemistry* **1989**, *28* (8), 3211−3220.
(36) Holmgren, A.; Reichard, P. *Eur. J. Biochem.* **1967**, *2* (2), 187−196.
(37) Neue, G.; Dybowski, C. *Solid State NMR* **1997**, *7* (4), 333−336.
(38) Bielecki, A.; Burum, D. P. *J. Magn. Reson. Ser. A* **1995**, *116* (2), 215−220.
(39) Vangorkom, L. C. M.; Hook, J. M.; Logan, M. B.; Hanna, J. V.; Wasylishen, R. E. *Magn. Reson. Chem.* **1995**, *33* (10), 791−795.
(40) Wishart, D. S.; Bigam, C. G.; Yao, J.; Abildgaard, F.; Dyson, H. J.; Oldfield, E.; Markley, J. L.; Sykes, B. D. *J. Biomol. NMR* **1995**, *6* (2), 135−140.
(41) McDermott, A.; Gu, Z. T. In *Encyclopedia of Nuclear Magnetic Resonance*; Grant, D. M., Harris, R. K., Eds.; Wiley: New York, 1996; Vol. 1, pp 1137−1147.
(42) Markley, J. L.; Bax, A.; Arata, Y.; Hilbers, C. W.; Kaptein, R.; Sykes, B. D.; Wright, P. E.; Wuthrich, K. *Pure Appl. Chem.* **1998**, *70* (1), 117−142.
(43) Takegoshi, K.; Nakamura, S.; Terao, T. *Chem. Phys. Lett.* **2001**, *344*, 631−637.
(44) Detken, A.; Hardy, E. H.; Ernst, M.; Meier, B. H. *Chem. Phys. Lett.* **2002**, *356* (3−4), 298−304.
(45) Baldus, M.; Petkova, A. T.; Herzfeld, J.; Griffin, R. G. *Mol. Phys.* **1998**, *95* (6), 1197−1207.
(46) Verel, R.; Baldus, M.; Ernst, M.; Meier, B. H. *Chem. Phys. Lett.* **1998**, *287* (3−4), 421−428.
(47) Delaglio, F.; Grzesiek, S.; Vuister, G. W.; Zhu, G.; Pfeifer, J.; Bax, A. *J. Biomol. NMR* **1995**, *6* (3), 277−293.
(48) Goddard, T. D.; Kneller, D. G. *SPARKY 3*; University of California: San Francisco, CA.
(49) Cornilescu, G.; Delaglio, F.; Bax, A. *J. Biomol. NMR* **1999**, *13* (3), 289−302.
(50) Pauli, J.; van Rossum, B.; Forster, H.; de Groot, H. J. M.; Oschkinat, H. *J. Magn. Reson.* **2000**, *143* (2), 411−416.
(51) Martin, R. W.; Zilm, K. W. *J. Magn. Reson.* **2003**, *165* (1), 163−174.
(52) Williams, J. C.; McDermott, A. E. *Biochemistry* **1995**, *34* (26), 8309−8319.
(53) Gu, Z. T.; Drueckhammer, D. G.; Kurz, L.; Liu, K.; Martin, D. P.; McDermott, A. *Biochemistry* **1999**, *38* (25), 8022−8031.
(54) Wishart, D. S.; Sykes, B. D. *J. Biomol. NMR* **1994**, *4* (2), 171−180.
(55) Ishii, Y. *J. Chem. Phys.* **2001**, *114* (19), 8473−8483.
(56) Castellani, F.; van Rossum, B.-J.; Diehl, A.; Rehbein, K.; Oschkinat, H. *Biochemistry* **2003**, *42*, 11476−11483.
(57) Hohwy, M.; Rienstra, C. M.; Jaroniec, C. P.; Griffin, R. G. *J. Chem. Phys.* **1999**, *110* (16), 7983−7992.
(58) Baldus, M.; Meier, B. H. *J. Magn. Reson.* **1997**, *128* (2), 172−193.
(59) Takegoshi, K.; Nakamura, S.; Terao, T. *J. Chem. Phys.* **2003**, *118* (5), 2325−2341.
(60) Crocker, E.; Patel, A. B.; Eilers, M.; Jayaraman, S.; Getmanova, E.; Reeves, P. J.; Ziliox, M.; Khorana, H. G.; Sheves, M.; Smith, S. O. *J. Biomol. NMR* **2004**, *29* (1), 11−20.
(61) Kraulis, P. J. *J. Appl. Crystallogr.* **1991**, *24*, 946−950.
(62) Merritt, E. A.; Bacon, D. J. *Methods Enzymol.* **1997**, *277*, 505−524.
(63) Merritt, E. A.; Murphy, M. E. P. *Acta Crystallogr. D* **1994**, *50*, 869−873.